Key Engineering Materials
ISSN: 1662-9795, Vol. 1057, pp 103-110
doi:10.4028/p-bGig86

Submitted: 2025-09-27
Revised: 2026-01-08
Accepted: 2026-01-31
Online: 2026-05-21

An Improved Analytical Model for SiC P-i-N Diode Reverse Recovery

Giorgian Borca-Tasciuc[1,a*] and T. Paul Chow[1,b]

[1]Rensselaer Polytechnic Institute, Troy, New York 12180, U.S.A.

[a*]borcag2@rpi.edu, [b]chowt@rpi.edu

Keywords: analytical modeling, reverse recovery, P-i-N diodes.

Abstract. We generalize a recent Si P-i-N reverse-recovery (RR) model to more accurately capture 4H-SiC diode behavior by adding deep-acceptor-limited anode injection, strong recombination (due to >100x shorter optimized high-level lifetimes compared to Si), and improved modeling of the depletion layer dynamics. Closed-form expressions for the growth of the depletion layer are derived, enabling analytical estimates for Q_{RR}, t_{RR}, and J_{PR}. The model is validated against Sentaurus RR simulations of optimized 4H-SiC P-i-N diodes spanning BV = 6–17kV and di/dt = 10 A/µs–10 kA/µs, achieving an average reduction in error of >90% for estimations of key switching performance parameters (Q_{RR}, t_{RR}, J_{PR}). By correctly capturing the dependence of Q_{RR} on di/dt, the model enables better estimates for the high-level lifetime (τ_{HL}) directly from the RR waveforms. The differential form enables straightforward utilization of the model to analyze non-idealized RR waveforms. Overall, the generalized model reveals a more favorable Q_{RR}–V_F trade-off than implied by the unmodified Si model and improves first-order device optimization prior to full design.

Introduction

Bipolar P-i-N junction diodes have a distinct BV-V_F trade-off compared to unipolar Schottky diodes due to conductivity modulation, in which the concentration of mobile carriers in the drift region can be increased well beyond the background doping. 4H-SiC P-i-N diodes are expected to have a lower V_F than 4H-SiC Schottky barrier diodes past 10kV. Recent advancements in reducing the lifetime-killing $Z_{1/2}$ defect and in suppressing the bipolar degradation phenomenon have eliminated some of the major impediments to realizing optimized 4H-SiC P-i-N diodes [1,2]. However, bipolar devices have a trade-off between the static and dynamic performance, as the on-state losses can be reduced at the expense of increasing the switching losses through an increase in Q_{RR} by increasing the degree of conductivity modulation. The total loss is minimized by trading off between the two losses. An analytical model allows a good first-order optimization of this trade-off before further refinement.

In [3], an analytical model is recently proposed to model the dynamics of Si P-i-N diode reverse recovery (RR) and estimate key switching performance parameters such as Q_{RR}, the snappiness factor t_B/t_A, and the reverse recovery time t_{RR}. However, several material aspects of SiC limit the applicability of this model: (1) the necessity of using deep acceptors reduces the injection efficiency of the anode, and (2) carrier recombination significantly reduces Q_{RR} due to the >100x reduction in the optimized high-level lifetime compared to Si. We thus generalize the model in [3] in order to increase its applicability to include SiC. We have evaluated the improvement in our model by performing simulations and evaluating the reduction in error obtained by the new model compared to the model in [3], and obtained substantial improvements in accuracy. The model indicates (and simulations confirm) that 4H-SiC P-i-N diodes have an improved BV-V_F trade-off than implied by the previous model. Our new model is expected to have applicability in enabling the design of competitive SiC P-i-N diodes and in improving the estimation of material parameters from the RR waveform.

Methodology

On-State.

Due to Aluminum being a deep-acceptor in 4H-SiC, <10% of electrically active acceptors are ionized at room temperature (RT). The space-charge neutrality equation can be used to determine the free hole concentration:

$$p + N_D^+ - n - N_A^- = 0$$

where:

$$p = N_V \exp -\frac{E_F - E_V}{kT},\ n = N_C \exp -\frac{E_C - E_F}{kT},\ N_A^- = \frac{N_A}{1 + g_A \exp\frac{E_A - E_F}{kT}},\ N_D^+ = \frac{N_D}{1 + g_D \exp\frac{E_F - E_D}{kT}}$$

An acceptable approximation of the solution to this transcendental equation for the hole-density in anode is given by:

$$p_{0P+} = \frac{N_\zeta}{2}\left(\sqrt{1 + \frac{4N_A}{N_\zeta}} - 1\right)$$

where:

$$N_\zeta = \frac{N_V}{\exp\frac{E_A - E_V}{kT}}$$

Equivalent expressions can be obtained for the free electron concentration n_{0N+} in the cathode, with $E_A - E_V$ replaced by $E_C - E_D$, and N_A replaced by N_D which will give satisfactory approximations if 100% donor activation cannot be assumed. Bandgap narrowing is modeled by assuming that:

$$E_A - E_V = \Delta E_{A0} - \alpha N_A^{\frac{1}{3}}$$

The parameter of interest is average carrier concentration n_a in the drift region. Using [3], this can be written as:

$$J_F = J_{SP+} n(-d)^2 + \frac{2qn_a d}{\tau_{HL}} + J_{SN+} n(+d)^2$$

$$J_{SP+} = \frac{qD_{nP+}}{p_{0P+} L_{nP+} \tanh\left(\frac{W_{P+}}{L_{nP+}}\right)}$$

$$J_{SN+} = \frac{qD_{pN+}}{n_{0N+} L_{pN+} \tanh\left(\frac{W_{N+}}{L_{pN+}}\right)}$$

D_{nP+}, D_{pN+} are the diffusion coefficients in the anode and cathode; L_{nP+}, L_{pN+} are the diffusion lengths in the anode and cathode; and W_P, W_N are the thicknesses of the anode and cathode, respectively. The thickness and high-level lifetime of the drift region is given as $t = 2d$ and τ_{HL}. $n(-d)$ and $n(+d)$ are the plasma concentration at the anode and cathode, and are given by the catenary carrier distribution:

$$n(x) = \frac{\tau_{HL}}{2qL_a}\left(\frac{\cosh\left(\frac{x}{L_a}\right)}{\sinh\left(\frac{d}{L_a}\right)} - B\frac{\sinh\left(\frac{x}{L_a}\right)}{\cosh\left(\frac{d}{L_a}\right)}\right)$$

Where $L_a = \sqrt{D_a \tau_{HL}}$ is the ambipolar diffusion length in the drift region, and $B = \frac{\mu_n - \mu_p}{\mu_n + \mu_p}$.

Thus, given the forward current density and the structural and material parameters of the P-i-N diode, the plasma carrier concentration $n_a$can be derived.

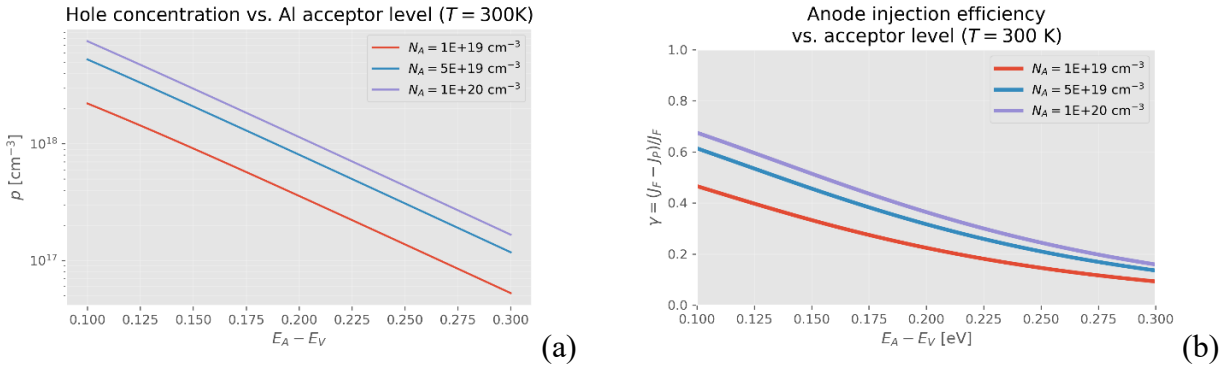

Fig. 1. Effect of aluminum acceptor level on (a) hole concentration and (b) anode injection efficiency.

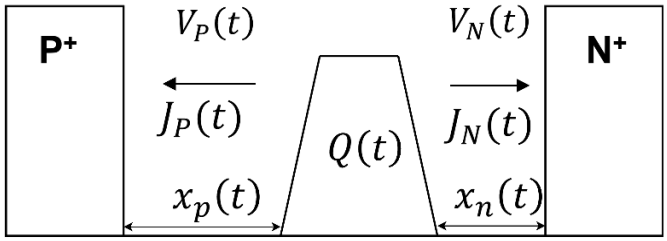

Fig. 2. Schematic representation of the drift region and modeled parameters during reverse recovery.

Dynamic Switching.

Figure 2 gives a schematic overview of the parameters solved by the dynamic switching equations. During the RR, holes are extracted at the anode and electrons are extracted at the cathode. The growth of the depletion region at the P^+ side is due to electrons in the plasma moving towards the cathode, leaving behind a depletion layer in which the holes are extracted towards the anode at saturation velocity. Given the small nature of $\frac{dn(x)}{dx}$ in the plasma, it can be assumed that electrons in the plasma are driven towards the cathode by drift. As the total current is given by:

$$J = J_F - at = q(\mu_n + \mu_p)n(x,t)E$$

We can approximate the electric field by assuming $n(x,t) \approx n_a(t)$ where n_a(t) is the average carrier density of the plasma at time t and thus derive:

$$E = \frac{J_F - at}{qn_a(t)(\mu_n + \mu_p)}$$

Thus, the electron current component, $J_n = q\mu_n nE$ becomes:

$$J_n = \frac{\mu_n}{\mu_n + \mu_p}(J_F - at)\frac{n(x,t)}{n_a(t)}$$

Again, assuming $n(x,t) \approx n_a(t)$, this simplifies to:

$$J_n = \frac{\mu_n}{\mu_n + \mu_p}(J_F - at)$$

We now apply a charge control approach to derive $\frac{dx_n}{dt}$. During an infinitesimal time step, the charge extracted at the boundary of the P^+/n- depletion region with the plasma is:

$$Q_n = J_n dt = \frac{\mu_n}{\mu_n + \mu_p}(J_F - at)dt$$

During this infinitesimal time step, the depletion region grew dx_n. Thus, the charge removed, assuming $n(x,t) \approx n_a(t)$ is:

$$Q_n = dx_p q n_a(t)$$

This yields, for dx_p/dt:

$$\frac{dx_p}{dt} = -\frac{\mu_n}{\mu_n + \mu_p}\frac{J_F - at}{qn_a(t)}$$

An acceptable approximation for $n_a(t)$, the average plasma concentration within the region that remains conductivity-modulated, can be made by assuming that $n_a(t)$ only changes through recombination. Thus, $n_a(t) = n_a e^{-\frac{t}{\tau_{HL}}}$, where n_a is simply the static value of the average carrier concentration of the plasma in the on-state. This yields the final formula for the growth of the depletion region at the P^+/n^- region:

$$\frac{dx_p}{dt} = -\frac{\mu_n}{\mu_n + \mu_p}\frac{J_F - at}{qn_a e^{-\frac{t}{\tau_{HL}}}}$$

Similar arguments made for the N^+/n^- depletion region yield:

$$\frac{dx_n}{dt} = -\frac{\mu_p}{\mu_n + \mu_p}\frac{J_F - at}{qn_a e^{-\frac{t}{\tau_{HL}}}}$$

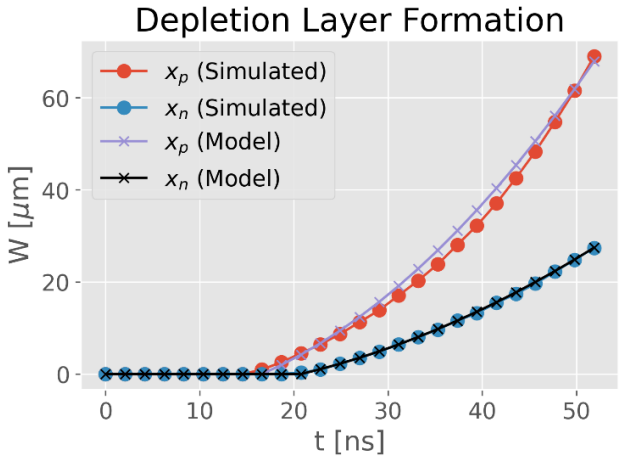

Fig. 3. Simulated depletion layer formation with μ_n/μ_p=2.5 along with model predictions.

An interesting observation is that this model predicts that the ratio of the depletion region widths x_p/x_n asymptotically approaches μ_n/μ_p, regardless of whether the diode is a P^+-n-N^+ diode or a P^+-p-N^+ diode. This effect can be seen in Figure 3, where RR was simulated with an exaggerated μ_n/μ_p to demonstrate the two-sided depletion formation.

The above-derived differential equations have the solution:

$$x_p(t) = C_p\tau_{HL}\left[(J_F + a\tau_{HL})\left(\exp\left(\frac{t_{1,p}}{\tau_{HL}}\right) - \exp\left(\frac{t}{\tau_{HL}}\right)\right) - a\left(t_{1,p}\exp\left(\frac{t_{1,p}}{\tau_{HL}}\right) - t\exp\frac{t}{\tau_{HL}}\right)\right], t > t_{1,p}$$

$$x_n(t) = C_n\tau_{HL}\left[(J_F + a\tau_{HL})\left(\exp\left(\frac{t_{1,n}}{\tau_{HL}}\right) - \exp\left(\frac{t}{\tau_{HL}}\right)\right) - a\left(t_{1,n}\exp\left(\frac{t_{1,n}}{\tau_{HL}}\right) - t\exp\frac{t}{\tau_{HL}}\right)\right], t > t_{1,n}$$

Where $C_p = \frac{\mu_n}{(\mu_n+\mu_p)qn_a}$ and $C_n = \frac{\mu_p}{(\mu_n+\mu_p)qn_a}$. The variables $t_{1,p}$ and $t_{1,n}$ denote when the depletion regions start growing at the P^+/n^- side and the N^+/n^- side, respectively. At $t = t_{1,p}$, there is no voltage across the P^+/n^- junction, and equivalently for $t = t_{1,n}$. Electric-field dependent mobilities, $\mu_n(E)$ and $\mu_p(E)$ can be used in the differential equations if the carriers in the plasma begin approaching their saturation velocity during the switching.

We now find the time $t_{1,p}$ and $t_{1,n}$ when the depletion region begins growing on each side. At time $t_{1,p}$, the carrier concentration at the anode/drift-region boundary is 0. Let b be the distance from the anode where the on-state equilibrium carrier concentration remains undisturbed. Then, at time $t_{1,p}$ current right at the anode is driven purely by diffusion. Using these assumptions and the previous derivations result in the following equations for the hole current exiting the anode at time t_1, p, where $\gamma = \frac{dn}{dx}|_{x=-d}$:

$$J_p(t_{1,p}) = \frac{\mu_p}{\mu_n + \mu_p}(J_F - at_{1,p}) = qD_P\frac{dn}{dx} \approx qD_p\frac{n(-d) - \gamma b}{b}$$

The total charge removed, utilizing the current zero-crossing $t_0 = \frac{J_F}{a}$ and approximating the removed charge using a triangle, is:

$$Q_{1,P} = \int_{t_0}^{t_{1,p}}(J_F - at)dt = \frac{1}{2}bqn(-d)$$

Thus, two equations are derived for two unknowns, $t_{1,p}$ and b. Combining the two equations yield a rather unwieldly cubic polynomial, whose positive real root is the time the voltage across the P^+/n^- junction is equal to zero. Equivalent arguments yield $t_{1,n}$. We utilize $t_1 = \min(t_{1,p}, t_{1,n})$, as the moment the depletion layer begins growing on one side, the voltage will promptly cross zero.
We now have all the terms to derive a straightforward expression for the voltage supported across the P-i-N diode during the RR:

$$V_{AK}(t) = V_P(t) + V_N(t)$$

Where $V_P(t)$ is the voltage supported across the P^+/n^- junction and $V_N(t)$ is the voltage supported across the N^+/n^- junction. Using Poisson's equation, $V_P(t)$ and $V_N(t)$ can be straightforwardly derived from $x_n(t)$ and $x_p(t)$:

$$V_P(t) = \frac{1}{2\epsilon_s}\left(\frac{at - J_F}{v_{sat,p}} + qN_D\right)x_p(t)^2$$

$$V_N(t) = \frac{1}{2\epsilon_s}\left(\frac{at - J_F}{v_{sat,n}} + qN_D\right)x_n(t)^2$$

The peak reverse current is obtained by solving for $V_{AK}(t_2) = V_S$. To model the final phase of the RR, consider the charge remaining in the drift region once J_{PR} is reached:

$$Q_r \approx qn_a \exp\left(-\frac{t}{\tau_{HL}}\right)(2d - x_n(t_2) - x_p(t_2) - h_n - h_p)$$

Here, h_p and h_n are the slopes of the carrier profile at the boundary of the P^+/n^- depletion region of the plasma, and at the boundary of the N^+/n^- depletion region and the plasma, respectively. The expression for these are derived from the diffusion current at the boundary of the plasma at time t_2:

$$J_n = \frac{\mu_n}{\mu_n + \mu_p}J_{PR} = qD_n\frac{dn}{dx} \approx qD_n\frac{n_a \exp -\frac{t}{\tau_{HL}}}{h_n}$$

The expression for h_p is equivalent. At this point, we assume that recombination is negligible in extracting the remaining charge. This is a justifiable assumption as once the large peak reverse current is reached, it becomes more efficient at removing charge than recombination. Our simulations confirm this assumption. A tail-like decay is still seen in the final phase of inductive switching, but this is due to the decay of the diffusion gradient as carriers exit the conductivity-modulated region, not due to carrier recombination. With this assumption in hand, we can write:

$$\frac{1}{2}J_{PR}t_b = Q_r$$

And thus, the total reverse recovery charge, Q_{RR} can be written as:

$$Q_{RR} = \frac{1}{2}(t_2 + t_b - t_0)J_{PR}$$

The expression for t_b assumes a linear decay of the current from J_{PR} to 0. A satisfactory waveform for the current decay can be derived by assuming for $t > t_2$:

$$J(t) = J_{PR} \exp\left(-\frac{t - t_2}{\tau_b}\right), t > t_2$$

The current-decay time constant τ_b, capturing the effects of the decay of the gradients driving diffusion, can be defined using:

$$\int_{t_2}^{\infty} J(t) = Q_r$$

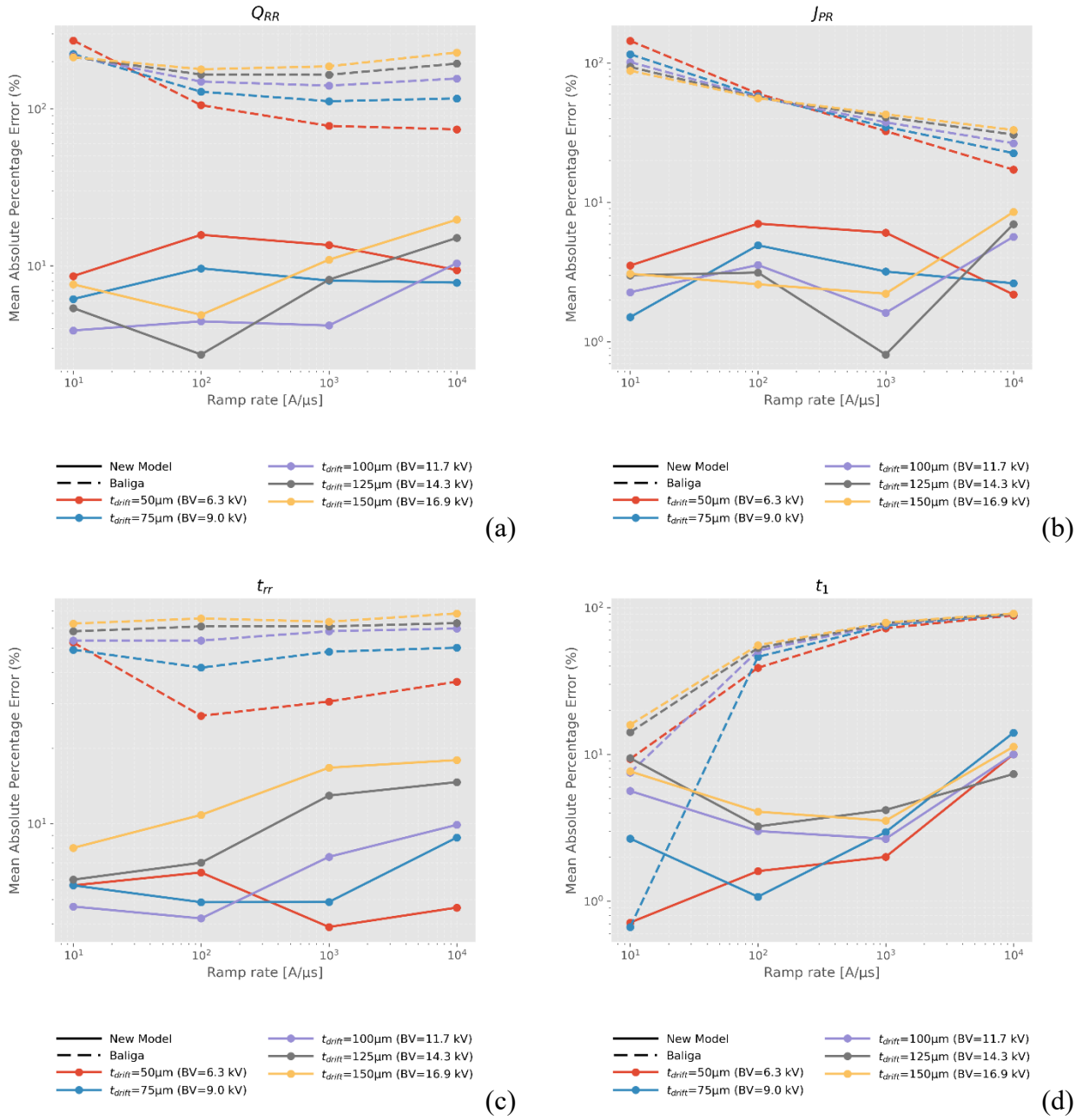

Fig. 4. Errors in model predictions for (a) Q_{RR}, (b) J_{PR}, (c) t_{RR}, and (d) t_1. Error displayed in log-scale.

Model Verification

TCAD Sentaurus is used to perform simulations in order to verify the model. Optimized 4H-SiC p-i-n diodes are designed with differing mid-region thicknesses varying from 50µm to 150µm by 25µm increments, yielding breakdown voltages (BV) between 6kV and 17kV. Inductive-load RR simulations are performed on the optimized diodes, varying the ramp rate between 10A/µs and 10kA/µs and the reverse voltage from 1/8 to ½ the BV. The key switching parameters ($Q_{RR,sp}$, J_{PR}, t_{RR}, t_I) are extracted and quantitatively compared with the model predictions using the prediction error ($\frac{x_{true}-x_{predicted}}{x_{true}}$). The mean absolute percentage error (MAPE) is used to aggregate the errors across the different switching reverse voltage. The model described in [3] is used as a baseline.

As is visible in Figure 3, the model makes substantial improvements over the Si RR model. Both J_{PR} and Q_{RR} are accurate always accurate within 20% across the 60 tested scenarios and are almost always within 10%. The average errors are 8.8% for Q_{RR} (94% reduction), 3.7% for J_{PR} (93% reduction), 9.2% for t_{RR} (84% reduction), and 5.3% for t_I (90% reduction). This testifies to the degree of relative as well as absolute accuracy of the new model. Figure 4 provides a qualitative comparison of the new model, the simulation results, and the model described in [3].

The increase in the error of t_{RR} with increasing ramp rate arises from the increased role of recombination in removing the remaining charge (Q_r) in the final phase.

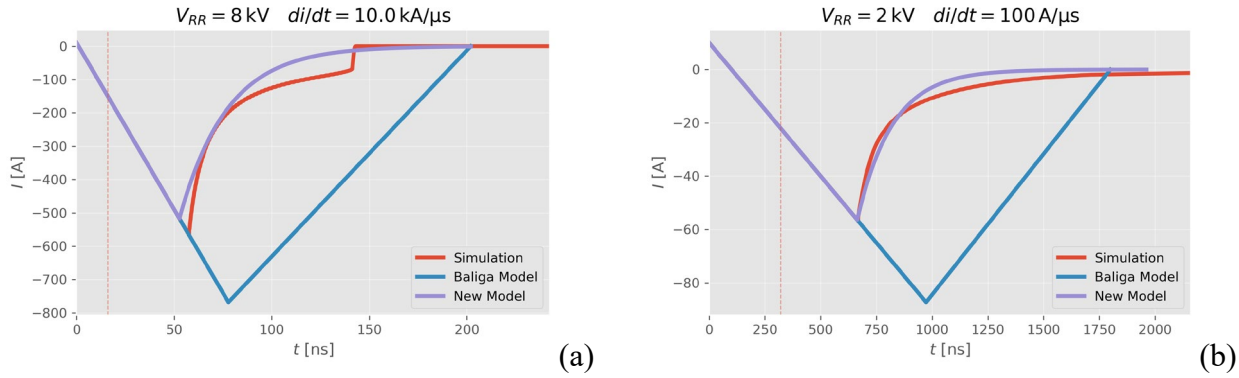

Fig. 5. Representative examples of simulated waveforms vs model predictions.

The new model can be used to make accurate Q_{RR}-V_F curves, as is seen in Figure 6(a). Usage of the model in [3] provides an excessively pessimistic Q_{RR}. Thus, the performance of the 4H-SiC P-i-N diode is significantly better than predicted by [3]. Figure 7(b) demonstrates that the model can also reproduce the dependence of Q_{RR} on di/dt. The same τ_{HL} extracted in [4] using the slope of the I_F-Q_{RR} curve also gives a reasonable fit for the Q_{RR}-di/dt curve. As current waveforms during switching often deviate from the idealized form assumed for modeling, the differential forms can be used with $J(t)$ substituting for $J_F - at$ when using the model for device characterization.

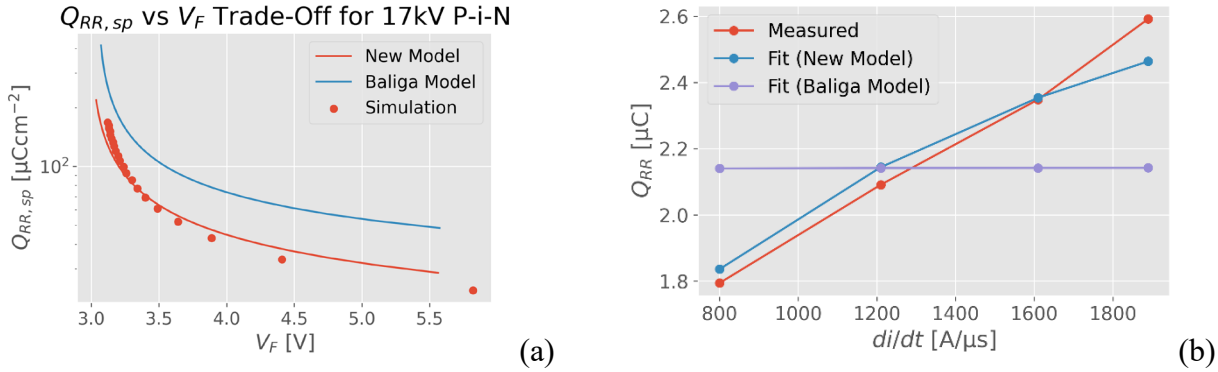

Fig. 6. Comparisons of models for (a) Q_{RR}-V_F trade-off curves, and (b) Q_{RR}-di/dt curve. Experimental data from [4].

Table 1. Important parameters utilized in RR simulations.

E_{A0}	α	N_A	N_D	E_C-E_D	$\mu_{n,max}$	$\mu_{p,max}$
0.265eV[5]	3.6E-8eVcm	1E19cm^{-3}	1E19cm^{-3}	0.1eV	950cm^2/V-s	125cm^2/V-s

Conclusion

We generalized the classical Si reverse-recovery framework presented in [3] by including reduced anode injection efficiency due to utilization of deep acceptors, recombination during RR, and two-sided depletion growth. We utilize the model to predict RR in optimized 4H-SiC P-i-N diodes, deriving closed-form relations for depletion growth and analytical estimates of Q_{RR}, t_{RR}, and J_{PR} that match Sentaurus RR across BV = 6–17 kV and di/dt = 10 A/µs–10 kA/µs, reducing errors by >90% versus the unmodified Si model. The model predicts an improved Q_{RR}-V_F trade-off than the previous model, extending the regions in which 4H-SiC P-i-N diodes become competitive. The model reproduces the dependence of Q_{RR} on di/dt seen in empirical RR measurements. The differential form of the model enables utilization of the model with a measured (non-idealized) RR current waveform to analyze the stored charge in the drift region. Thus, the model expands the viable design space for SiC P-i-N diodes by guiding τ_{HL} and drift-layer sizing against V_F-Q_{RR} and can be utilized to obtain additional insight into measured RR waveforms, accelerating device design and characterization.

References

[1] M. Kato, O. Watanabe, T. Mii, H. Sakane, S. Harada, "Suppression of stacking-fault expansion in 4H-SiC PiN diodes using proton implantation to solve bipolar degradation," *Sci. Rep.* 12 (2022) 18790.

[2] T. Okuda, G. Alfieri, T. Kimoto, J. Suda, "Oxidation-induced majority and minority carrier traps in n- and p-type 4H-SiC," *Appl. Phys. Express* 8 (2015) 111301.

[3] B.J. Baliga, *Fundamentals of Power Semiconductor Devices*, 2nd ed., Springer, Cham, 2019.

[4] K. Nakayama, S. Ogata, T. Hayashi, T. Hemmi, A. Tanaka, T. Izumi, K. Asano, D. Okamoto, Y. Tanaka, T. Mizushima, M. Yoshikawa, H. Fujisawa, K. Takenaka, M. Takei, Y. Yonezawa, K. Fukuda, H. Okumura, "High voltage and fast switching reverse recovery characteristics of 4H-SiC PiN diode," *Mater. Sci. Forum* 778–780 (2014) 841–844.

[5] A. Koizumi, J. Suda, T. Kimoto, "Temperature and doping dependencies of electrical properties in Al-doped 4H-SiC epitaxial layers," *J. Appl. Phys.* 106 (2009) 013716.